INSIGHTS INTO THE EFFECT OF SPATIAL VARIABILITY OF RECORDED EARTHQUAKE GROUND MOTION ON THE RESPONSE OF A BRIDGE STRUCTURE

By

Ali Güney ÖZCEBE, Chiara SMERZINI and Vishvendra BHANU

ABSTRACT

With the aim of evaluating the effect of spatial variability of recorded ground motions on spatially extended structures, we present a numerical study on the linear and non-linear response of an idealized integral-abutment bridge, subject to the 2004 Parkfield recordings at the UPSAR array. The results show that spatial variability of recorded motion may present features which are poorly predictable by standard coherency approaches and this may have a considerable impact even on a regular, 300-m long structure on homogenous stiff soil conditions, leading to localized increase or decrease of engineering demands parameters up to a factor of about 50%.

Keywords: spatial variability of ground motion; strong-motion recordings; fiber-based numerical modeling, non-linear time history analyses; Eurocode 8

1. INTRODUCTION

Earthquake-resistant design and assessment of structures are conventionally performed assuming that they are subjected to the same input motion at the foundation level. As a matter of fact, the largest dimension of most structures is usually small enough compared to the wavelength of incoming seismic waves that the ground motion can be reasonably assumed to be the same at each point of the structure itself. However, for civil engineering structures which extend over significant distances, such as bridges, viaducts and lifeline systems, earthquake ground motions arriving at different points of the structure may vary significantly both in amplitude and phase. In such cases consideration of the spatial variability of earthquake ground motion (SVEGM) is crucial to accurately estimate the structural seismic response. For this reason, for Eurocode 8, EC8 – Part 2 [CEN, 2005a], as well as for the 2008 Italian Building Code, NTC08 [CS.LL.PP., 2008], a spatially varying seismic action has to be taken into account for the design of bridges under certain conditions.

Evidences of damage to lifeline structures, such as pipelines and highway bridges, during past earthquakes (e.g. M_w 6.7 1971 San Fernando, M_w 6.9 1989 Loma Prieta, M_w 6.9 1995 Kobe and M_w 6.3 1999 Chi-Chi earthquakes), pointed out that significant differential movements associated with asynchronous input motion can lead to an excessive increase of seismic demand and contribute, at least partially, to structural failure [Tzanetos et al., 2000; Elnashai et al., 1995; Zerva et al., 1988].

After over three decades of studies, it is nowadays well recognized that SVEGM may have detrimental effects on the structural response, causing displacement patterns along the structure and/or strength/ductility demands which are almost unpredictable owing to the multi-parametric nature of wave propagation and of its interaction with different structural elements. After the first pioneering research studies in the middle 1960s, when structures were studied in the linear range and the SVEGM was considered only in terms of delay in the arrival time at the supports [see e.g. Bogdanoff et al., 1965; Johnson and Galletly, 1972], the installation of dense instrument arrays and the development of spatial coherency models [see e.g. Harichandran and Vanmarcke, 1986; Abrahamson. et al., 1991; Luco and Wong, 1986; Der Kiureghian, 1996] gave rise to an increasing interest on the issues related to the effect of spatially variable excitations on the response of a large variety of structural systems [for a comprehensive overview see Zerva, 2009]. Among the different classes of structures under

investigation (e.g., pipelines, tunnels, dams, etc..), the structural configuration which has gained an increasing research interest because of its diffusion is that of bridges. This is the structural typology considered in this work.

Only to cite few among the most important and recent contributions, the work of Monti et al. [1996] is one of the first extensive numerical studies addressing the issues of asynchronous motion in terms of wave passage effects on the linear and non-linear response of different bridge models. The study concluded that, while in linear models spatial variable input motion is beneficial with respect to the synchronous case, localized increase and decrease of ductility demand may result from multi-support excitation in non-linear analyses and that synchronous input motion leads to a conservative design.

Saxena et al. [2000] reached different conclusions investigating the effects of the three main sources of spatial incoherence, i.e., wave passage effect, incoherence effects and local site conditions (homogenous vs heterogeneous soil types at bridge supports), on the non-linear response of two bridge structures. The authors found that the assumption of uniform support excitation, the standard case in design practice, is not conservative, especially in case of different soil conditions at the bridge supports, leading to differences in terms of peak pier ductility demand of about a factor of two.

Two recent studies on the inelastic response of bridges, including structural irregularities, are by Sextos et al. [2003a; b] and Lupoi et al. [2005]. In the first study an extensive parametric study on the inelastic response of 20 bridges under multi-support excitation, including effects of heterogeneous soil conditions and soil-foundation-superstructure interaction (SSI) effects, pointed out that relative pier displacements are strongly tied to the overall length of the bridge and asynchronous motions should be considered beyond a threshold length of 400 m. Furthermore, it was found that neglecting input motion variability, associated not only with time delay and loss of coherency but also with local site amplification and SSI interaction, may provide unsafe estimates for the ductility demand by a factor of 25% on average and up to a factor of 3 in the extreme case. The role of foundation flexibility and variable local site conditions has been further highlighted in a number of studies, see e.g. Capatti et al. [2015] and Sextos et al. [2015].

Based on the analysis of a wide set of 200-m long idealized bridges, Lupoi et al. [2005] showed that, also for this relatively short bridge length, the effects of incoherence may

affect considerably the structural response, increasing the ductility demand at the base section of the piers. Further, researchers found that the probability of failure systematically grows with the geometrical irregularity of the structures.

Referring to the latter point, in particular to the case of curved bridges, Sextos et al. [2004] studied the response of a real curved bridge structure, i.e., the Krystallopigi Bridge in Greece, for a set of asynchronous earthquake scenarios accounting for the wave passage effect alone as well as the combined effect of wave passage and incoherence. The analyses pointed out that asynchronous response (pier top displacements and base moments) in the transverse direction is up to twice the synchronous one owing to wave passage effects. Combining the wave passage and the loss of coherency effects, the response in terms of pier base bending moment in the transversal direction in almost unpredictable because, depending on the variable character of the motion, the asynchronous response leads from a reduction up to 70% to an increment exceeding the 100% with respect to the fully coherent case. In-plane bridge irregularity is found to play a significant role also in the recent work of Šavor Novak et al. [2015], where the spatial variability of ground motion turns out to have an unfavorable effect on the response of most of the considered design values in a short 100-m span reinforced concrete (RC) arch bridge, with maximum deviations from the synchronous case of a factor larger than 3.

Referring to the design of seismic control systems for the vibration control of cable-stayed bridges, Abdel Raheem et al. [2010] found that SVEGM, measured only in terms of wave passage effect, may induce an increase of force response and cable deviation parameters.

From this literature review, it is evident that, while a variety of bridge models have been investigated to evaluate the impact of SVEGM on the structural response and its implications for seismic design, one of the aspects often neglected regards the features of seismic input and its consistency with evidences from ground motion recordings obtained at dense arrays. As a matter of fact, the vast majority of research studies make use of artificial stochastic time histories satisfying a prescribed spatial coherency model [e.g. Luco and Wong, 1986], under the simplifying assumptions of a common target power spectrum for all bridge supports and standard values of apparent velocity. However, little attention has been paid to the verification of the impact of considering a set of closely spaced strong motion

recordings, thus fully preserving the actual spatial coherency structure of earthquake ground motion.

Therefore, at variance with previous studies the results of which may be conditioned on the specific assumptions of the spatial coherency model, the original aim of this work is to study the impact of the spatial variability of seismic input on a bridge structure by considering direct application at the different foundation points of earthquake ground motion recordings obtained from a dense array network during a strong earthquake. For this purpose, a regular, idealized RC bridge, belonging to the class of the integral abutment bridges, was considered. The main geometric and structural features of the bridge are inspired by the Humboldt Middle Channel Bay Bridge, in California (USA). Considering an integral abutment bridge is expected to increase the impact of SVEGM on its seismic response, because the lack of joints makes it more sensitive to differential movements of the ground. As for the spatially variable seismic input, the near-field recordings obtained at the dense US Geological Survey Parkfield Seismograph Array (UPSAR) array during the M_W6 September 28th 2004 Parkfield earthquake, were considered, upon a suitable spatial interpolation procedure to adapt the phase and amplitude of records to the actual position of the foundation points.

A wide spectrum of dynamic time histories analyses has been carried out through fiber-based structural modeling in SeismoStruct [Seismosoft, 2016], under different assumptions regarding the features of input motion (synchronous vs spatially variable) and the behavior of the structure (linear vs non-linear). The results of the full dynamic time history analyses were compared with the ones obtained following one of the most advanced code-based approaches for evaluating the effects of SVEGM, like the one in EC8. Finally, aspects related to the comparison with standard time delay approaches as well as to the dependence on the alignment of record set, have been addressed.

2. OVERVIEW OF SPATIAL VARIABILITY OF EARTHQUAKE GROUND MOTION

2.1 Theoretical background on spatial coherency

The spatial variability of ground motion is attributed to three different factors [see e.g. Kramer, 1996; Harichandran, 1999]: (i) wave passage effect, arising from differences in the

arrival times of seismic waves at separate stations on ground surface; (ii) incoherence effect (extended source + ray-path), arising from differences in the manner of superposition of waves (a) arriving from an extended source, especially in the near-source region, and (b) scattered by irregularities and heterogeneities along the path from the source to the site; (iii) local site effects, arising from differences in local sub-surface soil conditions at each station, which may alter the amplitude and frequency content of seismic waves propagating from the bedrock to the ground surface.

The common approach to quantify SVEGM for engineering applications is the evaluation of the spatial coherency function, which describes the joint spectral features of ground motions at two generic locations on ground surface [for a thorough overview see Zerva, 2009]. Specifically, given a pair of motions, $a_j(t)$ and $a_k(t)$, at two discrete locations j and k separated by a distance d, the spatial coherency is defined as follows:

$$\gamma_{jk}(f,d) = \frac{S_{jk}(f,d)}{\sqrt{S_{jj}(f) \cdot S_{kk}(f)}} \tag{1}$$

where: f is the frequency, $S_{jj}(f)$ and $S_{kk}(f)$ are the smoothed power spectral density of $a_j(t)$ and $a_k(t)$, respectively; $S_{jk}(f,d)$ is the smoothed cross spectrum between $a_j(t)$ and $a_k(t)$. The coherency function of Eq. (1) is a complex function, whose absolute value, $0 \leq |\gamma_{jk}(f,d)| \leq 1$, is termed lagged coherency. The lagged coherency is the most commonly used coherency measure in engineering application and measures, at each frequency f, the extent to which data recorded by two stations at distance d are correlated.

Engineering models of SVEGM are usually calibrated from strong-motion dense array recordings during past earthquakes (e.g. SMART-1, Lotung Taiwan; UPSAR Array, Parkfield, California USA, which has been used in this work). Several spatial coherency functions, both semi-empirical and empirical, have been proposed on the basis of the random vibration theory [see e.g. Luco and Wong, 1986; Somerville et al 1988; Der Kiureghian, 1996] as well as of regression fitting of an analytical function to empirical coherency estimates [see e.g. Harichandran and Vanmarcke, 1986; Abrahamson et al., 1991; Ancheta et al., 2011]. Because of its clarity and simplicity, the Luco and Wong [1986] model, referred to hereafter as LW86, has been the most used in engineering studies addressing the effect of SVEGM on the dynamic response of long structures. It gives the following expression for the lagged coherency:

$$|\gamma(f,d)| = \cdot exp[-(\alpha \cdot 2\pi f \cdot d)^2] \quad (2)$$

where α is the coherency drop parameter controlling the exponential decay of the coherency with distance and frequency, with a median value of $2.5 \cdot 10^{-4}$ s/m, as suggested by the authors.

2.2 Code-based approaches

EC8-Part 2 and NTC08 are ones of the few seismic codes worldwide to define a procedure to take into account the spatial variability of the seismic action for the design of bridge structures. On the other hand, most modern codes treat the problem only on the basis of seating length provisions, such as the U.S. Standard Specifications for Highways and Transportation Bridges [AASHTO, 1996] and ATC-32 [1996]. For a careful overview on current code provisions and guidelines, we refer the reader to Sextos and Kappos [2009]. In the following reference will be made to EC8.

According to EC8, the influence of spatial variability of ground motion shall be considered for bridges with continuous superstructure when one or both of the following two conditions hold: (i) soil properties along the bridge vary to the extent that more than one ground types correspond to the bridge supports; (ii) soil properties along the bridge are approximately uniform, but the length of the continuous superstructure exceeds the threshold length, L_{lim}. The latter is computed as $L_{lim} = L_g$ /1.5, where L_g is the distance beyond which the ground motion may be supposed to be completely uncorrelated and it depends on the ground type. The EC8 values of L_g (Table 3.1N of EC8-2) vary from 600 m to 300 m for soil classes from A (shear wave velocity in the top 30 m V_{S30}> 800 m/s) to D (V_{S30}< 180 m/s).

The approach proposed in the seismic norm to quantify the effect of spatially varying support excitations is based on the assumption that the response of a bridge can be expressed as the sum of two components: an inertial component (DY) and a pseudo-static component (PS). The former is the response of the bridge to the dynamic inertial forces under the standard hypothesis of synchronous input motion and can be determined by means of one of the analysis tools suggested by the code, e.g., a standard response spectrum analysis. On the other hand, the PS component is the static response of the bridge to suitable sets of differential displacements imposed at the supports of the structure. The displacement sets should reflect probable configurations of the spatial variability of the free-field seismic

motion and should be selected in such a way to induce maximum values of the effect of seismic action under investigation.

In EC8, two displacement sets, termed Sets A and B, shall be considered: (a) all piers are subjected to ground displacements of the same sign (positive or negative) but with varying amplitude (d_{ri}, see Eq. (3a)); (b) ground displacements occur in opposite directions at adjacent piers and, hence, the set consists of *absolute* displacements to be applied simultaneously but with opposite sign to all the supports (Δd_i, see Eq. (3b)). These displacements set are computed from the peak ground displacement d_g defined in EC8-Part 1 - §3.2.2.4 [CEN, 2004], based on the standard data defining the elastic design spectrum (such as PGA, site amplification factor and corner periods), as follows:

$$\text{Set A: } d_{ri} = \varepsilon_r \cdot L_i \le d_g \sqrt{2} \quad \text{with} \quad \varepsilon_r = d_g \sqrt{2} / L_g \tag{3a}$$

$$\text{Set B: } \Delta d_i = \pm \beta_r \cdot \varepsilon_r \cdot L_{av,i} \tag{3b}$$

where: i identify the support; L_i is the horizontal distance of support i from a reference support i_0; β_r is a factor depending on the homogeneity of soil conditions at adjacent supports (= 0.5 and 1 for uniform and non-uniform soil conditions, respectively); $L_{av,i}$ is the average of the distances $L_{i-1,i}$, $L_{i,i+1}$ of intermediate support i to its adjacent supports i-1 and i+1, respectively.

Finally, for each bridge direction, the most severe pseudo-static forces resulting from the application of the displacement sets A and B are then combined with the results of the inertial analysis using the standard Square-Root-of-Sum-of-Squares (SRSS) combination rule.

3. COHERENCY ESTIMATES FROM UPSAR RECORDINGS DURING THE 2004 PARKFIELD EARTHQUAKE

In this study, the near-source acceleration recordings provided by the UPSAR dense array during the M_w6.0 September 28th 2004 Parkfield event are considered, instead of artificial accelerograms compliant with a prescribed coherency model, to determine the multiple-support seismic excitation. Before presenting the numerical model of the bridge, in this Section an overview of the main features of spatial coherency of the 2004 Parkfield recordings at UPSAR is provided.

UPSAR is a dense array consisting of 14 irregularly spaced seismograph stations (S1-S14), with inter-station distances ranging from about 25 m up to 960 m, located on a stiff site

at a distance of approximately 12 km west of the 2004 Parkfield fault rupture [for a through overview see Fletcher et al., 1992; 2006]. The top panel of Figure 1 shows the layout of the twelve UPSAR stations which were operational during the 2004 event, while in the bottom panel the three-component acceleration time histories (East-West: EW; North-South: NS; Vertical: UD) recorded at the stations S11, S12 and S13 are illustrated. Note that these recordings will be the input data for the spatial interpolation procedure implemented in this work.

Estimates of the lagged spatial coherency (see Eq. (1)) are obtained from the 12 available recorded time series of ground acceleration, after proper synchronization of time series, through a standard spectral analysis [see Zerva, 2009]. Figure 2 shows the lagged coherency estimates from UPSAR recordings for 50 m wide distance bins in the range 0-300 m (which is approximately the length of the bridge analyzed) and for the three components of ground motion (EW, NS, UD). Note that for each distance bin the plotted coherency curve is the mean of the coherency curves over all possible pairs of stations belonging to the same bin. In the same figure, the UPSAR coherency estimates are compared with the LW86 model of Eq. (2) for a constant median value of the coherency drop parameter, namely $\alpha = 2.5 \cdot 10^{-4}$ s/m, as well with the model by Harichandran and Vanmarcke [1986], referred to as HV86 (valid for $d \geq 100$ m).

In agreement with the findings of Konakli et al. [2014], who studied in detail the spatial variability features of the 2004 Parkfield dataset, these results indicate that at small separation distances spatial coherency associated with UPSAR recordings may be lower than the ones provided by empirical models, while a reverse trend typically occurs at larger separation distance. It is also noted that a least-squares regression of LW86 model on these coherency estimates would results in α values which are far from being constant, as typically assumed, but depend on distance (α decreases for increasing inter-station distance). Such a loss of coherency for the Parkfield event may be related to the condition of proximity to the seismic fault, potentially coupled with other complex propagation effects (3D propagation, topography), which are not accounted for by standard coherency models.

To determine the seismic input at all bridge supports, a spatial interpolation of records was performed, with the aim of preserving the inherent coherency features of ground motion. Specifically, the bridge structure (that will be described in Section 4) is hypothetically

transferred to the UPSAR area in an orientation such that the left abutment (LA) is coinciding with station S13 and two piers, namely, P2 and P8, are coinciding with S12 and S11, respectively (see sketch of the conceptual model in Figure 1, top right panel). Then, the input motions below the remaining 10 piers of the bridge are found by linear spatial interpolation on the recorded displacement waveforms, being the latter obtained by double integration of corrected acceleration recordings (namely, high-pass filter with cut-off frequency of 0.05 Hz to remove unphysical drifts). In a nutshell, for an intermediate pier between any two reference piers with known displacements, the motion is computed as weighted average of reference displacements, with weights inversely proportional to the relative distance between the nodes. Only for the right abutment (RA) it was necessary to carry out an extrapolation by using the information provided by records S12 and S11. Finally, the accelerograms obtained at each pier by spatial interpolation are rotated appropriately (50 degrees clockwise) to get the input motions along the principal longitudinal (X) and transverse (Y) direction of the bridge.

The acceleration response spectra of the ground motions obtained at each bridge support are presented in Figure 3; in the same figure, the UPSAR recordings are also highlighted. A significant variability of input motions is found, especially on the transverse component and at periods coinciding with the fundamental vibration response of the bridge (see Section 5), which is also the most critical, most likely because it coincides with the direction normal to the fault of the Parkfield earthquake, along which near-field motion tends to polarize.

4. STRUCTURAL MODELING

In this work, an idealized bridge structure, inspired by the Humboldt Bay Middle Channel (HBMC) Bridge, in California (USA), is considered [see e.g. Zhang et al., 2008; Elgamal et al., 2008]. The bridge structure considered in this study is a 330-m long, 10-m wide and 12-m high nine span composite RC bridge with four precast and pre-stressed concrete I-girders and cast-in-place concrete slabs (see Figure 4). The nine bays have equal lengths of 36.67 m. Numerical models were constructed in SeismoStruct [Seismosoft, 2016] to take into account both linear and non-linear response of the bridge.

To focus on the effect of the SVEGM alone, an idealized jointless bridge system was considered with the following simplified modelling assumptions: (i) the superstructure system

is connected to the vertical supports as cast-in-situ without any connection elements or hinges; (ii) foundation-subsoil and abutment-backfill soil interaction phenomena are not modelled, by providing fixed restraints at base nodes. Hypothesis (i) is motivated by the fact that the HBMC is an integral abutment bridge without any type of classical bearings, instead the connections at superstructure level are maintained with shear keys and rebar nails with two expansion joints, whose non-linear effects have not been modelled herein. Referring to the second hypothesis, although it is recognized that SSI effects may play a relevant role [see e.g. Sextos et al. 2003b; 2004] and may be the key to explain the observed bridge response [Sextos et al., 2015], the nature of the UPSAR records, obtained on relatively stiff and homogenous soil conditions with limited evidences of local site effects [see Fletcher et al. 2006], justifies this assumption. This was also confirmed by additional numerical analyses accounting for linear elastic impedances at foundation level and nonlinear spring-gap element system for the abutment/backfill. In the following the longitudinal and transverse principal axes of the bridge will be denoted by X and Y, respectively.

4.1 Linear structural model

In the linear model, a symmetric uniaxial model is used to represent the cracked concrete cross-sections of the vertical members. The parameters of the constitutive and geometric model are summarized in Figure 4. Furthermore, a Rayleigh damping with 2% damping ratio in the frequency range 0.4–0.6 s, corresponding to the dominant vibration modes of the bridge (see eigenvalue analysis in Section 5), is assumed. The choice of a damping ratio of 2%, lower than the standard value of 5%, has been made for consistency purposes with the non-linear model (see Section 4.2).

4.2 Non-linear structural model

To model the initiation and spread of non-linearity with sufficient accuracy, piers and abutments are modeled through force-based elements [Spacone et al., 1996; Neuenhofer and Filippou, 1997] with 10 Lobatto integration sections. To cope with, instead, the distribution of plasticity within each cross-section, rectangular RC sections are discretized with 300 and 900 fibers for piers and abutments, respectively.

In the sections, whose geometries and reinforcement details are presented in Figure 4 and in Table 1, respectively, non-linear uni-axial behavior for concrete fibers are modelled with Mander confined concrete model [Mander et al., 1988] with cyclic reversals defined by Martinez-Rueda and Elnashai [1997]. Properties assigned to the Mander concrete models are: f'_c = 28 MPa (unconfined compressive strength); f_t = 2.2 MPa (tensile strength); E_c = 24870 MPa (modulus of elasticity of the uncracked concrete); ε_c = 0.002 (strain at peak strength). Nonlinearity in the steel fibers are modelled by using the constitutive relation of Menegotto-Pinto [Menegotto and Pinto, 1973]. Properties of steel layers are: $E_s = 2 \cdot 10^5$ MPa (modulus of elasticity of the reinforcement steel); f_{ys} = 415 MPa (yield strength); r = 0.008 (isotropic strain hardening parameter) and ε_{su} = 0.10 (fracture strain of the steel).

Finally, as in fiber-based modeling of non-linearity, a significant portion of the damping sources (such as material inelasticity, repetitive crushing/cracking) is inherently considered, Rayleigh damping corresponding to 2% damping ratio is provided [Correia et al., 2013].

4.3 Overview of numerical analyses

To study the impact of recorded asynchronous input, a wide set of Dynamic-Time History Analyses (DTHA) have been carried out for both linear (LS) and non-linear (NLS) model of the bridge, under the hypothesis of bi-directional horizontal input (X+Y), as listed in Table 2. To evaluate the beneficial or detrimental effect of asynchronous excitation, for each model, two classes of analyses are conducted: (i) synchronous motion analyses (referred to as SYN hereafter), and (ii) spatially variable motion analyses (SV).

For SYN analyses, it is worth underlining that, when actual recordings at multiple sites are adopted directly for asynchronous case, the definition of a "reference" synchronous seismic input is far from obvious owing to the variability of available input motions in terms of amplitude and frequency content [see thorough discussion in Sextos et al. 2015]. In this work, a single ground motion was selected as the closest one to the mean (unscaled) spectral acceleration response, in the range of periods around the fundamental longitudinal and transverse vibration periods of the bridge. In such conditions, the idealized uniform scenario is expected to induce approximately the same average modal forces as induced by the SV case. It turned out that the motion at the base of Pier P6 (i.e. node 7, referred to as gm7),

corresponds to average SYN scenario, see Figure 3 (a closer match is obtained for transverse component, where the impact of SVEGM is higher).

Furthermore, to investigate the impact of different asynchronous excitation models, the following cases have been considered:

- SV base hypothesis (A1): multiple support motions are derived from the set of UPSAR recordings S11-S12-S13 (alignment A1) through the spatial interpolation procedure described in Section 3. For this case, a complete path of numerical analyses, from DTHA to performance-based assessment through Incremental Dynamic Analyses (IDA) according to EC8 provisions, has been carried out. As explained previously, the reference SYN excitation is given by gm7;
- SV-Z: consideration of three-directional seismic input, by including the vertical motion (Z) in addition to the horizontal components (X+Y).
- SV-Time Delay (TD): standard time delay analysis by applying two representative values of apparent propagation velocity, i.e.: V_{a1}=2400 m/s (TD1) and V_{a2}=1000 m/s (TD2), on a single input time history;
- SV-A2: base bridge motions are determined from a second alignment of UPSAR recordings, A2=S08-S09-S10. Specifically, stations S08, S09 and S10 are made coincident with Right Abutment (RA), Pier P5 and Left Abutment (LA), respectively (see Figure 1). For this case, SYN analyses are obtained by applying to all bridge supports the ground motion at the base of Pier P4 (at node 5, i.e., gm5).

Referring to the vertical motion (SV-Z), it is recognized that vertical to horizontal response spectral ratios may be significant in the low period range especially in the near-source region of severe earthquakes [see e.g. Gulerce and Abrahamson, 2011; Bommer et al., 2011], which is the case of the Parkfield event considered in this study. Although a thorough investigation of the impact of vertical component on different engineering demand parameters is beyond the scope of this study and will be object of further research studies, we aim herein at providing only some preliminary insights into the potential effect of vertical asynchronous excitation during real near-fault earthquake scenarios.

The results of all the numerical analyses obtained for the base hypothesis of SYN vs SV motion will be illustrated in Sections 5 and 6, while in Section 7 the impact on different observationally-based SV models (SV-Z vs SV-TD vs SV-A2) will be discussed.

5. EFFECTS ON THE BRIDGE RESPONSE

Before addressing the impact of spatially varying input motion on the bridge response, the modal response properties of the structure are presented (see Table 3). As can be noted from the effective modal mass percentages, the response in longitudinal (X) direction is dominated by a single vibration mode, with a fundamental frequency of f_{1X}=1.8 Hz (mass participation factor =100%). On the other hand, the transverse (Y) response is multi-modal: besides the first mode at f_{1Y}=2.1 Hz, with percent mass participation=73.9%, further contributions are found from higher modes, mainly f_{2Y}=2.9 Hz and f_{5Y}=4.8 Hz, with mass participation factors of 7.0% and 16.9%, respectively. In Figure 5, the vibration mode shapes and corresponding mass participation factors are provided for selected translational modes.

5.1 Amplification function

Amplification function of pier response along the horizontal directions (longitudinal X or transverse Y) is computed in the frequency domain as the ratio of the Fourier transform of any response time history (acceleration/velocity/displacement) at a given point on the superstructure over the one of the corresponding base node. Figure 6 shows the longitudinal and transverse amplification functions for Pier P1 and P5 (top and bottom panel, respectively). These amplification curves also compared with the well-known amplification response curve of a Single-Degree-Of-Freedom (SDOF) system with longitudinal and transverse periods equal to 0.56 s and 0.48 s, respectively.

For both piers, the SYN and SV longitudinal response is rather similar to the one of a SDOF with f_n=f_{1X}=1.8 Hz, as the X response is fully governed by the first vibration mode. However, SV leads to perturbations at higher vibration frequencies, especially for P1, with minor effects on the dominant vibration mode. Furthermore, regardless of the presence of spatial variability, the amplification response at the deck level is almost the same from pier to pier because of the large axial stiffness of the deck.

Referring to the transverse (Y) amplification response which is multi-modal (f_{1Y}=2.1 Hz, f_{2Y}=2.9 Hz and f_{3Y}=4 Hz, see Table 3), as easily identifiable from the SYN response, overall, SV motion turns out to excite higher, mostly antisymmetric, modes of vibration, inducing a strong constructive interference at frequencies higher than about 2 Hz. This is in substantial agreement with previous works [see e.g. Tzanetos et al., 2000; Burdette et al., 2008; Sextos and Kappos, 2009]. Furthermore, a different behavior is clearly noted for the mid-span (P5) and end-span piers (P1). For the former, SYN and SV amplification functions show a certain degree of similarity, although SV response at fundamental mode is reduced of about 20% and moderate constructive interference effects are found at higher modes. On the other hand, for the pier closer to the left abutment (P1), SV turns out to induce a destructive interference at first mode, with a decrease of amplitude of about 30%, and to create significant amplifications especially in the range of frequencies between first and second modes, i.e., 2-3 Hz, as a result of the local dynamic response of the close-by abutment. Finally, it should be also noted that the input motions show a stronger spectral variability in transverse direction (see Figure 3) that contributes to the observed amplification characteristics, as well.

5.2 Peak structural response

The effect of spatial variability of ground motion on the peak structural response is evaluated in terms of relative deck displacement (with respect to the base) and shear force for selected elements, namely piers P1, P5 and P8. Results are presented in a compact format using synthesis plots, where the *x*-axis values correspond to the results of SV analyses and the *y*-axis values are from the SYN analyses, both for linear and non-linear models. Using this graphical representation, alignment of values along the bisecting 1:1 line means that SV ground motion response does not affect the response. Moreover, the 1:1.50 and 0.67:1 dashed lines correspond to 50% reduction and 50% increment, respectively, in the peak response due to SV ground motion. Solid markers represent the results from the non-linear model (NLS) while hollow markers are for the linear model (LS).

Figure 7 illustrates the variations of peak relative displacement values (D_x and D_y). Referring to the linear longitudinal response, it is found that relative peak displacements are unbiasedly distributed around 1:1 line, meaning that SV hypothesis does not have any impact on results owing to the dominant contribution of first vibration mode. However, when non-linear effects are accounted for, SV motion tends to increase the displacement demand of a

factor between 30-40%. This factor decreases passing from P8 to P1, exactly in the order of decreasing intensity of input ground motion, due to induced non-linearity on the pier elements, which share the same deck displacement demand but are subjected to different input base motion. As highlighted previously, the effect of SVEGM is apparent on the transverse direction, where localized increase (end-span piers) and decrease (central piers) of displacement demands, up to a factor of 50%, occur owing to the constructive interference at higher modes and reduction of vibration amplitude at the fundamental mode, respectively. The difference in terms of displacement values are also due to different stiffness characteristics of linear and non-linear structural systems (i.e. for linear model, cracked stiffness is used, for non-linear model true stress-strain relations are provided), that make the non-linear model behaves slightly stiffer when mild non-linearity is present in the section.

Similar conclusions apply to the maxima of the shear force (V), see Figure 8: while longitudinal response is poorly affected by asynchronous motion, except an increase of about 20% in non-linear SV analyses, the impact of SVEGM is very significant on bridge transverse response, ending up with 50% decrease of the base shear for mid-span piers and 50% increase for end-span piers with respect to the synchronous case.

5.3 Total base shear time histories

Total base shear time histories have been selected as a parameter indicating the global structural response when subjected to spatially variable input motion. Instead of only the maxima, full time histories of total base shear (both X and Y components) are provided in Figure 9 for both linear (top) and non-linear (bottom). For linear case, the impact of spatial variability is apparent on the response along transverse (Y) direction, along which piers are not constrained as strongly as they are in longitudinal (X) direction, leading to a reduction of maximum base shear of a factor of about 2, because of decrease of modal forces in the first vibration mode. For non-linear case, the transverse global response is strongly reduced due to energy dissipation associated with non-linear effects and the impact of spatial variability turns out to be more limited, as compared to the linear response, at least under the considered SYN scenario. However, when dealing with spatially variable seismic actions, local element demand parameters, such as chord rotation (see following discussion), play a more important role than global parameters like total base shear and should be addressed.

6. EUROCODE 8-BASED CONSIDERATIONS

The aim of this Section is to compare the results of full linear dynamic analyses with the ones obtained by applying the simplified but rational EC8 approach for a spatially variable seismic action (see Section 2.2). Although, by definition, the pseudo-static EC8 approach cannot account for the excitation of higher modes, such a comparative analysis is considered useful to test the degree of applicability of code prescriptions when actual SV recordings are used.

For this purpose, the inertial (DY) component is obtained from the LSSYN analysis (see Table 2), under the assumption of a classical 5% Rayleigh damping (instead of 2%), and comparison is analyzed in terms of pier shear forces (V_Y) along the transverse direction, where the impact of SVEGM turns out to be predominant. To carry out the PS analyses under differential displacement sets A and B (PS-A and PS-B, respectively; see Eqs. (3a) and (3b)), the following parameters are assumed: design peak ground displacement d_g = 0.08 m, associated with a peak ground acceleration a_g= 3.2 m/s^2, corresponding roughly to the average value of the 10 input motion (see Figure 3); EC8 site class B, applicable to UPSAR array, where shear velocity is about 400 m/s [Fletcher et al., 1992]; limiting length L_g = 500 m; homogenous soil conditions β_r = 0.5; $L_{av,I}$ = 36.67 m (all spans are of equal length). Under these assumptions, Eqs. (3a) and (3b) lead to: $\varepsilon_r = 2.263 \cdot 10^{-4}$ and $\Delta d = 4.15 \cdot 10^{-3}$ m. Note that the bridge length (330 m) is nearly coincident with the threshold L_{lim} = 333 m, above which the effect of SV excitation should be considered according to EC8 provisions. It is found that PS-B is slightly more critical for all piers and, therefore, is the one considered in the combination with the effects of DY synchronous analysis.

In agreement with what considered in previous analyses, the DY analyses have been performed considering as input the ground motion with spectral features approaching the mean response spectrum, i.e., gm7 ("LSSYN-avg"). The maximum pier shear forces are then obtained combing the results of these two analyses with the PS ones through the SRSS rule.

The comparison, shown in Table 4, indicates that the EC8 approach provides unbiased estimates, close, on average, to the values obtained from full asynchronous dynamic analysis, although maximum differences of about 40% and 50% can be found on the lower and higher side, respectively. The resulting performance of EC8 approach is somehow worse than the results reported in literature for analogous, regular, bridge configurations on uniform soil

conditions [see Sextos and Kappos 2009], mainly because of the peculiar, strong, variability pattern of the seismic excitation under consideration. Furthermore, it worth underlining that this comparison is somehow conditioned on the specificity of the single scenario adopted for the analyses and more general conclusions could be drawn by including further recordings.

In addition to this comparison, Appendix A presents the assessment of seismic performance of the bridge for different EC8 limit states through IDA by increasing the original demand of both SYN and SV motions by scale factors from 1.5 up to 6.

7. EFFECT OF DIFFERENT HYPOTHESES ON SV INPUT

This Section aims at providing some insights into the impact of different hypotheses regarding the SV seismic input on the non-linear response of the bridge, namely: (i) inclusion of vertical component (X+Y vs X+Y+Z); (ii) time delay (TD) analyses with two constant values of apparent propagation velocity, i.e. V_{a1}=2400 m/s (TD1) and V_{a2}=1000 m/s (TD2) (SV vs TD); (iii) choice of UPSAR record set to determine the multiple support excitations (SV-A1=S11-S12-S13 vs SV-A2=S08-S09-S10). Referring to (ii), the choice of V_{a1}=2400 m/s is dictated by the findings of Fletcher et al. [2006], who performed a spatial correlation analyses of the 2004 Parkfield records, while V_{a2}=1000 m/s is derived from previous studies focusing on earthquake-induced ground strains [Paolucci and Smerzini, 2009]. In the following, the chord rotation maxima θ^{max} is considered as engineering demand parameter to assess the impact of SV input motions.

For the purpose of (i), similarly to the horizontal components, vertical components (Z) of UPSAR records are first spatially interpolated to determine the motion at each support of the bridge and then scaled by 1.5, 2.5 and 6 scale factors in SV IDA analyses. Figure 10 shows the ratios of θ^{max} obtained from three-component input motion (X+Y+Z) over those obtained considering only horizontal motion (X+Y) for all piers and abutments. Again, vertical motion affects predominantly the bridge transverse response and variability of results starts being appreciable for scale factors higher than 1.5. However, the largest effects, occurring in the abutments, turn out to be limited to 10%. For some elements of the bridge, a slight beneficial effect is also found when large levels of non-linearity are accounted for.

The comparison with TD analyses (point ii) is illustrated in Figure 11, where the ratios of the θmax from either the SYN, TD1, TD2 analyses over the ones from the SV computations are provided (A1 alignment is considered). It is noted that:

- referring to the transverse behaviour (rotations around X axis), SYN analyses tend to overestimate the response at mid-piers and underestimate the response at end-piers. On the other hand, SYN leads to lower rotations around the Y axis owing to the slightly smaller spectral demand of SYN motions at the vibration period range of the bridge;
- under the assumption of a value of apparent velocity specific for the study area (i.e. V_a=2400 m/s – TD1), TD analyses provide some improvements with respect to SYN, by limiting the extent of underpredictions and overpredictions in some structural elements.

Finally, to address the issues related to the sensitivity of results to the record set, Figure 12 illustrates the chord rotation ratios from both TD analyses over the ones from the SV scenario, under the assumption of record set A2, deployed according to a different azimuth with respect to the seismic source. It is found that, while for A1 assumption of V_a=2400 m/s provides a closer match with the reference SV analysis, for A2 a reverse trend is obtained, being V_a=1000 m/s more suitable to describe the actual asynchronous response along the longitudinal direction. Along the transverse direction, V_a=2400 m/s still provides more precise estimates, suggesting suggests that two different values of apparent velocity are suitable for longitudinal and transverse bridge response, respectively. For the former response, although the selection of the reference SYN scenario plays an important role, such differences are interpreted to be also associated with the conditions of proximity to the seismic source, where larger phase differences of seismic waves are expected to occur along the direction which is roughly perpendicular to the fault strike (see sketch on the right hand side of Figure 12). This suggests that, in near fault conditions, local site conditions are not the only factor affecting apparent velocity but orientation of the bridge together with directionality of fault rupture may play a role. Further studies including the analysis under different near-fault datasets will help strengthen this observation.

8. SUMMARY AND CONCLUSIONS

This work addresses the issues related to the impact of spatial variability of ground motion, as obtained from actual closely-spaced earthquake recordings, on the dynamic response of bridge structures. As a target, an idealized integral abutment bridge structure was considered, both because of its widespread diffusion also in seismic regions, and because of its sensitivity to differential displacements owing to its jointless structural features. At variance with the vast majority of studies which use as asynchronous seismic input artificial stochastic time histories compliant with a prescribed spatial coherency model, we derived the multiple-support excitation by spatial interpolation of the near-field recordings provided by the UPSAR dense array during the M_W6 September 28th 2004 Parkfield earthquake.

A set of linear and non-linear dynamic time histories analyses was performed using fiber-based numerical modeling to evaluate whether such asynchronous seismic input is beneficial or detrimental in terms of EC8-based engineering demand parameters, such as chord rotations and shear forces.

For the idealized regular 330-m long bridge under study, the most salient results can be summarized as follows:

(i) SVEGM turns out to affect predominantly the response of the bridge along the transverse direction, as, contrary to the longitudinal response which is governed by a single vibration mode, it tends to strongly excite higher, mostly antisymmetric, vibration modes for all piers;

(ii) Overall, asynchronous input motion leads to localized amplification (end-span piers) or de-amplification (mid-span piers) of structural demands, by factors up to 50%, due to the strong constructive interference effects at higher vibration modes, and reduction of amplification at the fundamental vibration period, respectively (as apparent from the bridge deck amplification function of Figure 6);

(iii) For this particular set of ground motions, comparison with the EC8 approach provides average unbiased predictions, although maximum differences between 40-50% are found both on safe and unsafe side at selected piers, owing to the inability of pseudo-static method to predict the contribution of higher modes as well as the location of

structural elements which are favorably or unfavorably affected by spatially variable seismic actions (Table 4);

(iv) Under the assumption of a proper value of apparent propagation velocity, conventional time domain analyses may provide slightly improved predictions with respect to synchronous analyses, although they cannot reproduce the actual variability of seismic action at the foundation level (Figure 11). Furthermore, the selection of a proper value of apparent velocity, which is recognized to be very critical in simplified engineering approaches [see e.g. Pitilakis and Paolucci, 2007], is even less straightforward in near-source conditions, as it may depend on the orientation of the bridge with respect to the seismic fault (see Figure 12). This suggests that, in the near-fault region of major earthquakes, the apparent velocity may be governed not only by the local soil conditions but also the relative source-bridge position.

Although these conclusions are limited to only one integral abutment structural type and to a specific set of strong motion recordings, they raise the point of a more in-depth evaluation of the impact of SVEGM, because the complexity of earthquake ground motion, especially in the proximity of the seismic source, may induce significant effects, even on a regular, 330-m long bridge on homogenous stiff ground conditions. For this reason, future research will be addressed to include the analysis of further dense array recordings (e.g. 2004 Parkfield event at Turkey Flat Array; M_W 6.5 San Simeon earthquake at UPSAR) and different structural configurations (e.g. joint-type bridges). Finally, results points out the relevance of a careful analysis of the relationship between the input excitation and higher vibration modes to get accurate prediction of the impact of SVEGM and to identify the most affected structural elements.

ACKNOWLEDGEMENTS

This work has been funded by Italian Department of Civil Protection in the framework of the 2014-2016 ReLUIS RS2 Project entitled "*Numerical simulations and near-source effects*". Authors wish to warmly thank Roberto Paolucci and Lorenza Petrini for a series of fruitful

discussions which contributed to improve the overall quality of the work. The comments and suggestions of three anonymous reviewers are also acknowledged.

REFERENCES

AASHTO, American Association of State Highway and Transportation Officials [1996] Standard Specification for Highway Bridges (16th edition).

Abdel Raheem, S.E., Hayashikawa, T., Dorka, U. [2011] "Ground motion spatial variability effects on seismic response control of cable-stayed bridges," Earthquake Engineering and Engineering Vibration, 10(1),37-49

Abrahamson, N.A., Schneider, J.F. and Stepp, J.C. [1991] "Empirical spatial coherency functions for application to soil-structure interaction analyses," *Earthquake Spectra* 7(1), 1–27.

ATC, Applied Technology Council [1996] Improved Seismic Design Criteria for California Bridges: Provisional Recommendations: ATC-32. National Bureau of Standards: Washington, DC.

Ancheta, T.D., Stewart, J.P. and Abrahamson, N.A. [2011] "Engineering characterization of earthquake ground motion coherency and amplitude variability," *Proceedings of the 4th IASPEI/IAEE International Symposium on the Effects of Surface Geology on Seismic Motion*, Santa Barbara, USA.

Bogdanoff, J.L., Goldberg, J.E. and Schiff, A.J. [1965] "The effect of ground transmission time on the response of long structures," *Bulletin of the Seismological Society of America* 55(3), 627–640.

Bommer, J.J., Akkar, S. and Kale, Ö [2011] "A Model for Vertical-to-Horizontal Response Spectral Ratios for Europe and the Middle East," Bulletin of the Seismological Society of America 101(4), 1783–1806.

Burdette, N.J., Elnashai, A.S., Lupoi, A., Sextos, A.G. [2008] "Effect of asynchronous earthquake motion on complex bridges. I: Methodology and input motion," *Journal of Bridge Engineering*, 13, 158–165. doi:10.1061/(ASCE)1084-0702 (2008)13:2(158).

Capatti, M. C., Carbonari, S., Dezi, F., Leoni, G., Morici, M., Silvestri, F., Tropeano, G. [2015] "Effects of Non-Synchronous Ground Motion Induced by Site Conditions on the Seismic Response of Multi-Span Viaducts," *6th International Conference on Earthquake Geotechnical Engineering*, 1-4 November 2015, Christchurch, New Zealand

CEN, European Committee for Standardization [2004] Eurocode 8: Design Provisions for Earthquake Resistance of Structures, Part 1.1: General Rules, Seismic Actions and Rules for Buildings.

CEN, European Committee for Standardization [2005a] Eurocode 8 - Design of structures for earthquake resistance - Part 2: Bridges.

CEN, European Committee for Standardization [2005b] Eurocode 8: Design of Structures for Earthquake Resistance. Part 3: Assessment and Retrofitting of Buildings.

Correia, A. A., Almeida, J. P. and Pinho, R. [2013] "Seismic energy dissipation in inelastic frames: understanding state-of-the-practice damping models," *Structural Engineering International* 23(2), 148-158.

CS.LL.PP. [2008] DM 14 Gennaio 2008. Norme tecniche per le costruzioni, Gazzetta Ufficiale della Repubblica Italiana, 29. (in Italian).

Der Kiureghian, A. [1996] "A coherency model for spatially varying ground motions," *Earthquake Engineering and Structural Dynamics* 25(1), 99–111.

Elgamal, A., Yan, L., Yang, Z. and Conte, J. P. [2008] "Three-dimensional seismic response of Humboldt Bay bridge-foundation-ground system," *Journal of Structural Engineering* 134(7), 1165-1176.

Elnashai, A.S., Bommer, J.J., Baron, C.I., Lee, D. and Salama, A.I. [1995] "Selected engineering seismology and structural engineering studies of the Hyogo-Ken Nanbu (Great Hanshin) earthquake of 17 January 1995", ESEE Research Report, No. 95-2, Imperial College of Science, Technology, and Medicine

Fletcher, J. B., Baker, L. M., Spudich, P., Goldstein, P., Sims, J. D. and Hellweg, M. [1992] "The USGS Parkfield, California, dense seismograph array: UPSAR," *Bulletin of the Seismological Society of America* 82(2), 1041-1070.

Fletcher, J. B., Spudich, P. and Baker, L. M.. [2006] "Rupture Propagation of the 2004 Parkfield, California, Earthquake from Observations at the UPSAR," *Bulletin of the Seismological Society of America* 96(4B), S129-S142.

Gulerce, Z. and Abrahamson, N. A. [2011] "Site-specific design spectra for vertical ground motion.," Earthquake Spectra," *Earthquake Spectra* 27(4), 1023-1047.

Harichandran, R.S. [1999] “Spatial variation of earthquake ground motion. What is it, how do we model it, and what are its engineering implications?,” Technical Report, Department of Civil and Environmental Engineering, Michigan State University.

Harichandran, R.S. and Vanmarcke, E. [1986] “Stochastic variation of earthquake ground motion in space and time,” *Journal of Engineering Mechanics ASCE* 112(2), 914–925.

Johnson, N.E. and Galletly, R.D. [1972] “The comparison of the response of a highway bridge to uniform ground shock and moving ground excitation,” *The Shock and Vibration Bulletin* 42, 75–85

Konakli, K., Der Kiureghian, A. and Dreger, D. [2014] “Coherency analysis of accelerograms recorded by the UPSAR array during the 2004 Parkfield earthquake,” *Earthquake Engineering and Structural Dynamics* 43(5), 641-659.

Kramer, S.L. [1996] Geotechnical Earthquake Engineering, Prentice Hall College.

Luco, J.E. and Wong, H.L. [1986] “Response of a rigid foundation to a spatially random ground motion,” *Earthquake Engineering and Structural Dynamics* 14(6), 891–908.

Lupoi, A., Franchin, P., Pinto, P.E. and Monti, G. [2005] “Seismic design of bridges accounting spatial variability of ground motion,” *Earthquake Engineering and Structural Dynamics* 34(4-5), 327-348.

Mander, J. B., Priestley, M. J. and Park, R. [1988] “Theoretical stress-strain model for confined concrete,” *Journal of Structural Engineering* 114(8), 1804-1826.

Menegotto, M. and Pinto, P. E. (1973) “Method of analysis for cyclically loaded rc frames including changes in geometry and non-elastic behaviour of elements under combined normal force and bending,” Report in *IABSE Congress Reports of the Working Commission* (vol. 13).

Martinez-Rueda, J.E. and Elnashai, A. S. [1997] “Confined concrete model under cyclic load,” *Materials and Structures* 30(3), 139-147

Monti, G., Nuti. C. and Pinto, P.E. [1996] “Non-linear response of bridges under multisupport excitation,” *Journal of Structural Engineering* 122(10), 1147-1159.

Neuenhofer, A. and Filippou, F.C. [1997] “Evaluation of nonlinear frame finite-element models,” *Journal of Structural Engineering* 123 (7), 958-966.

Paolucci, R. and Pitilakis, K. [2007] “Seismic Risk Assessment of Underground Structures under Transient Ground Deformations,” In *Earthquake Geotechnical Engineering.*

Geotechnical, Geological and Earthquake Engineering, Pitilakis K.D. (eds), vol 6, 433-459, Springer.

Paolucci, R. and Smerzini, C. [2008] "Earthquake-induced transient ground strains from dense seismic networks," *Earthquake Spectra* 24 (2), 453-470.

Šavor Novak, M., Lazarevic, D., Atalic, J. [2015] "Influence of spatial variability of ground motion on seismic response of bridges," *Gradevinar*, 67 (10), 943-957.

Saxena, V., Deodatis, G. and Shinozuka, M. [2000] "Effect of spatial variation of earthquake ground motion on the non-linear dynamic response of highway bridges," *Proceedings of the 12th World Conference on Earthquake Engineering*, Auckland, New Zealand.

Seismosoft [2016] "SeismoStruct 2016- A computer program for static and dynamic non-linear analysis of framed structures," online access: http://www.seismosoft.com.

Sextos, A.G., Kappos, A.J. and Pitilakis, K.D. [2003a] "Inelastic dynamic analysis of RC bridges accounting for spatial variability of ground motion, site effects and soil–structure interaction phenomena. Part 1: Methodology and analytical tools," *Earthquake Engineering and Structural Dynamics* 32 (4), 607-627.

Sextos, A.G., Kappos, A.J. and Pitilakis, K.D. [2003b] "Inelastic dynamic analysis of RC bridges accounting for spatial variability of ground motion, site effects and soil–structure interaction phenomena. Part 2: Parametric study," *Earthquake Engineering and Structural Dynamics* 32 (4), 629-652.

Sextos, A., Kappos, A. and Mergos, P. [2004] "Effect of soil-structure interaction and spatial variability on ground motion on irregular bridges," *Proceedings of the 13th World Conference on Earthquake Engineering*, Vancouver, B.C., Canada

Sextos, A.G. and Kappos, A.J. [2009] "Evaluation of seismic response of bridges under asynchronous excitation and comparisons with Eurocode 8-2 provisions," *Bulletin of Earthquake Engineering*, 7, 519–545.

Sextos, A.G., Karakostas, C., Lekidis, V., Papadopoulos, S.P. [2015] "Multiple support seismic excitation of the Evripos bridge based on free-field and on-structure recordings," *Structure and Infrastructure Engineering*, 11(11): 1510–1523. DOI: 10.1080/15732479.2014.977302.Somerville, P.G., McLaren, J.P., Saikia, C.K. and Helmberger, D.V. [1988] "Site-specific estimation of spatial incoherence of strong ground motion," *Proceedings Earthquake Engineering and Soil Dynamics II, recent*

advances in ground-motion evaluation, Geotechnical Special Pub No 20 ASCE, Park City, Utah, 188–202.

Spacone, E., Ciampi V. and Filippou F.C. [1996] "Mixed formulation of nonlinear beam finite element," *Computers and Structures* 58(1), 71-83.

Tzanetos, N., Elnashai, A.S., Hamdan, F.H and Antoniou, S. [2000] "Inelastic Dynamic Response of RC Bridges subjected to Spatial Non-Synchronous Earthquake Motion", *Advances in Structural Engineering* 3(3), 191-214.

Zerva, A., Ang, H.-S. and Wen, Y. K. [1988] "Lifeline response to spatially variable ground motions," *Earthquake Engineering and Structural Dynamics* 16(3), 361-379

Zerva A. [2009] Spatial variation of seismic ground motions. Modeling and engineering applications. CRC Press, Boca Raton.

Zhang, Y., Conte, J. P., Yang, Z., Elgamal, A., Bielak, J. and Acero, G. [2008] "Two-dimensional non-linear earthquake response analysis of a bridge-foundation-ground system," *Earthquake Spectra* 24(2), 343-386.

TABLES

Table 1 Reinforcement distributions and corresponding confinement factors for pier and abutment sections. Confined zone of the abutment sections is taken as 2 m. It is assumed that reinforcement detailing is conforming with seismic criteria.

Element type		Longitudinal Reinf. (Reinf. ratio ρ)	Lateral Reinf. Along depth	Lateral Reinf. Along width	Conf. factor
Pier		36ϕ32 (ρ~1%)	5 legs of ϕ14/100	3 legs of ϕ14/100	1.23
Abutment	Conf.	106ϕ32 (ρ~0.9%)	4 legs of ϕ14/100		1.28
	Unconf.		4 legs of ϕ14/100	-	1.00

Table 2 List of analyses performed. LS=Linear Structure; NLS = Non-linear structure; SYN=synchronous input motion; SV=spatially variable input motion; IDA=incremental dynamic analysis; TD=time delay analysis with apparent propagation velocity V_a. A1 refers to the set of UPSAR recordings S11-S12-S13, while A2=S08-S09-S10 (see Figure 1).

Analysis	Type of Analysis	Structural Model	Type of Loading (Component)	UPSAR Record Set	Time Delay V_a (m/s)
LSSYN	DTHA	Linear	SYN (X+Y)	A1	-
LSSV	DTHA	Linear	SV (X+Y)	A1	-
NLSSYN	DTHA	Non-Linear	SYN (X+Y)	A1	-
NLSSV	DTHA	Non-Linear	SV (X+Y)	A1	-
IDA NLSSYN	IDA	Non-Linear	SYN (X+Y)	A1	-
IDA NLSSV	IDA	Non-Linear	SV (X+Y)	A1	-
IDA NLSSV-Z	IDA	Non-Linear	SV (X+Y+Z)	A1	-
IDA NLSSV-TD1	IDA	Non-Linear	SV-TD1 (X+Y)	A1	2400
IDA NLSSV-TD2	IDA	Non-Linear	SV-TD2 (X+Y)	A1	1000
NLSSYN-A2	DTHA	Non-Linear	SYN (X+Y)	A2	-

NLSSV-A2	DTHA	Non-Linear	SV (X+Y)	A2	-
NLSSV-A2-TD1	DTHA	Non-Linear	SV-TD1 (X+Y)	A2	2400
NLSSV-A2-TD2	DTHA	Non-Linear	SV-TD2 (X+Y)	A2	1000

Table 3 Modal periods (*T*), frequencies (*f*) and corresponding modal mass percentages in global coordinates (m_i with *i*=X, Y, Z), from Eigenvalue Analysis.

Mode	T (s)	f (Hz)	m_X (%)	m_Y (%)	m_Z (%)
1X	0.56	1.79	100.0%	0.0%	0.0%
1Y	0.48	2.10	0.0%	73.9%	0.0%
2Y	0.34	2.94	0.0%	7.0 %	0.0%
3Y	0.21	4.04	0.0%	1.8%	0.0%
4Y	0.18	5.66	0.0%	0.4%	0.0%
5Y	0.07	4.81	0.0%	16.9%	0.0%
1Z	0.04	23.70	0.0%	0.0%	81.8%
2Z	0.02	45.55	0.0%	0.0%	18.2%

Table 4 Maximum transverse shear forces (V_Y) in the piers from: EC8 pseudo-static (PS) analysis under displacement sets A and B (PS-A and PS-B); LSSYN-avg: SYN linear DTHA with gm7 as input; EC8 predictions: $V_{Y,EC8}$ computed combining $V_{Y,PS-B} = max(V_{Y,PS-A}, V_{Y,PS-B})$ with $V_{Y,LSSYN-avg}$ with the SRSS rule; LSSV: linear DTHA with SV input.

Pier	$V_{Y,PS-A}$ (KN)	$V_{Y,PS-B}$ (KN)	$V_{Y,LSSYN-avg}$ (KN)	$V_{Y,EC8}$ (KN)	$V_{Y,LSSV}$ (KN)	$V_{Y,EC8}/V_{Y,LSSV}$ (-)
P1	184	214	1110	1130	1352	0.84
P2	208	261	1587	1608	2158	0.75
P3	210	247	2305	2318	2311	1.00
P4	209	246	2650	2661	1725	1.54

P5	209	246	2650	2661	1731	1.54
P6	209	247	2304	2317	2558	0.91
P7	210	261	1588	1609	2608	0.62
P8	204	214	1110	1130	1768	0.64

FIGURES

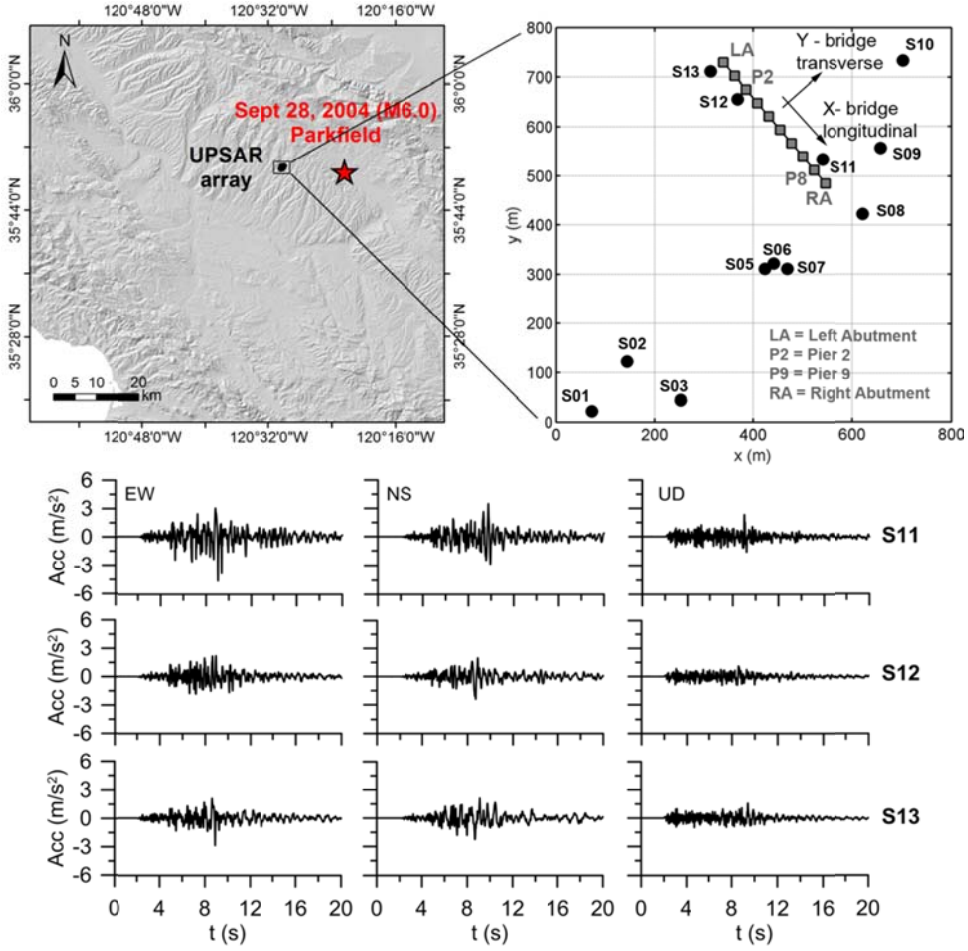

Figure 1 Top: location of the M_W6 Sept 28th 2004 Parkfield earthquake and layout of UPSAR array and of bridge model. Bottom: three-component (EW, NS and UD) acceleration time histories recorded at strong-motion stations S11, S12 and S13.

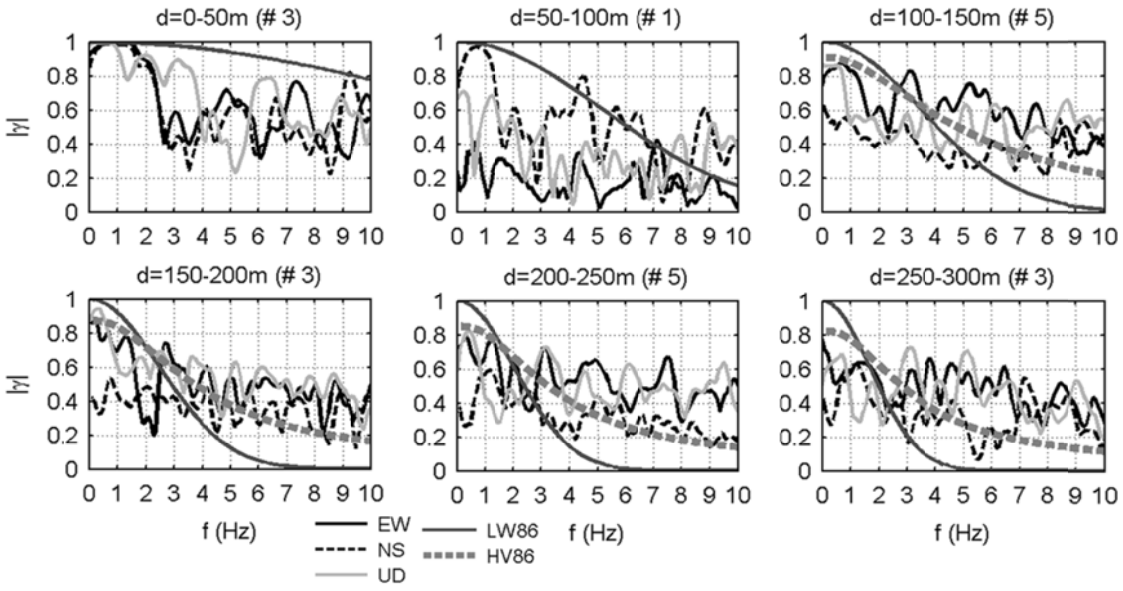

Figure 2 Mean lagged coherency estimates from UPSAR recordings (EW, NS and UD) during the Parkfield earthquake for 50 m wide distance bins form 0 to 300 m. The Luco and Wong [1986] - LW86 (α=2.5·10^{-4} s/m) and the Harichandran and Vanmarcke [1986] – HV86 models are also shown.

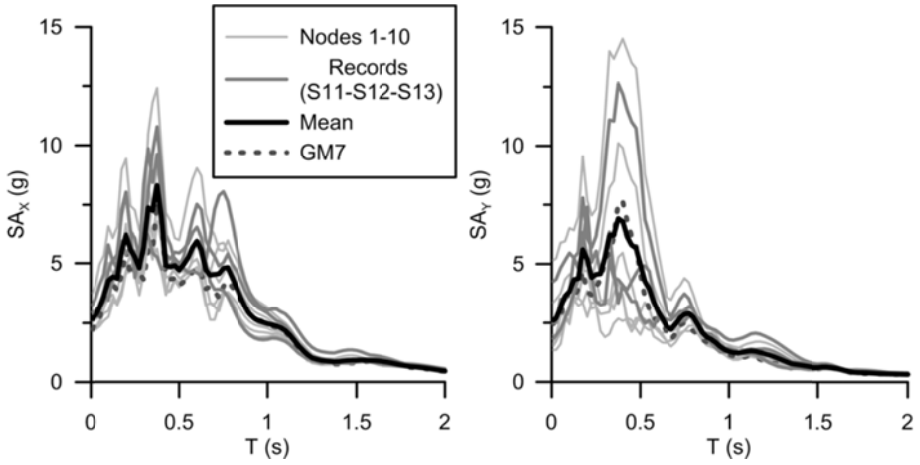

Figure 3 5% damped elastic acceleration response spectra of the 10 ground motions used as spatially variable input for bridge analyses, along the longitudinal X (left) and transverse Y (right) direction of the bridge.

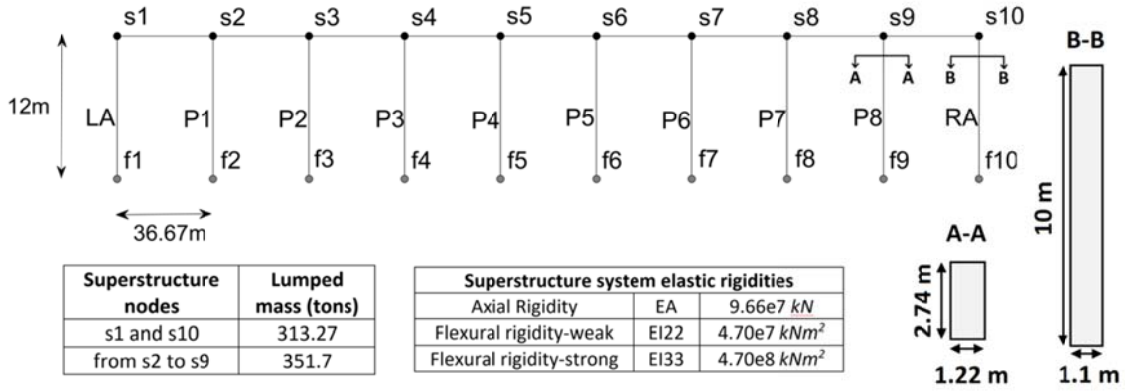

Superstructure nodes	Lumped mass (tons)
s1 and s10	313.27
from s2 to s9	351.7

Superstructure system elastic rigidities		
Axial Rigidity	EA	9.66e7 *kN*
Flexural rigidity-weak	EI22	4.70e7 kNm^2
Flexural rigidity-strong	EI33	4.70e8 kNm^2

Figure 4 The HBMC bridge model (LA=Left Abutment; RA=Right Abutment; P= Pier). A vertical exaggeration factor is applied for graphical purposes.

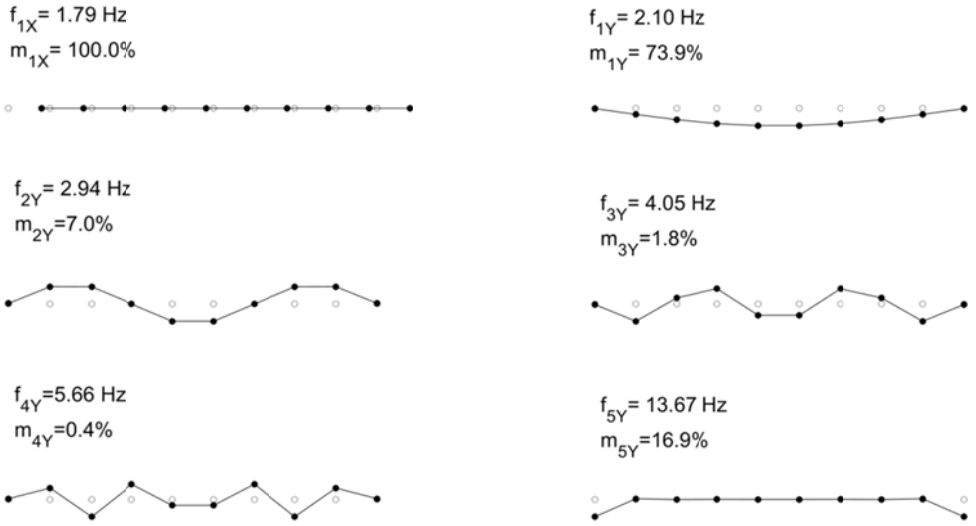

Figure 5 Vibration mode shapes (top view) corresponding to selected translational modes along the longitudinal (X) and transverse (Y) directions. Modal mass factors are also shown.

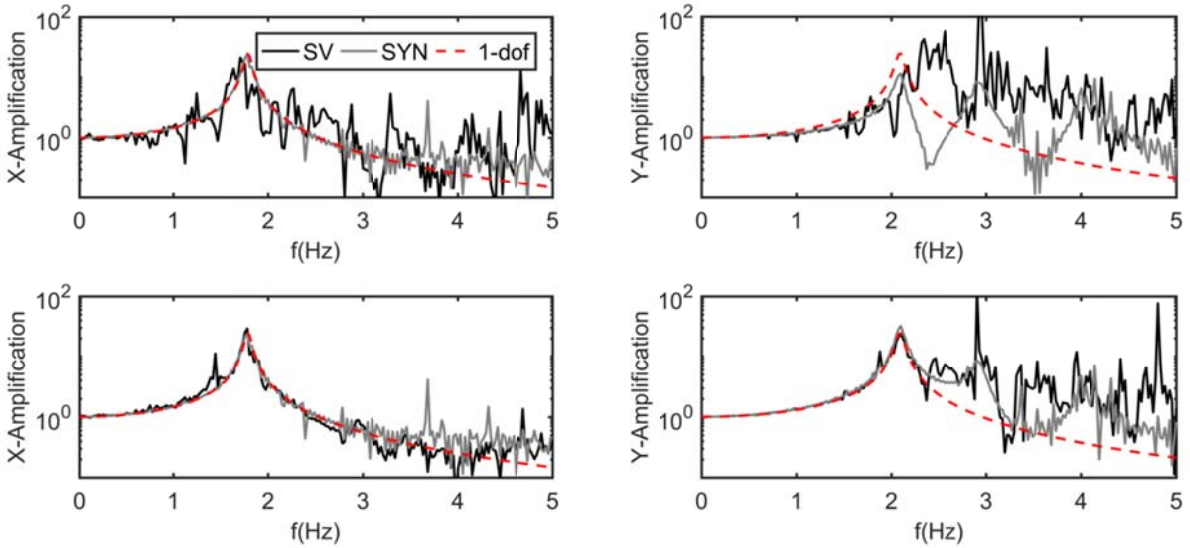

Figure 6 Deck amplification functions along longitudinal X (left) and transverse Y (right) direction for pier P1 (top) and P5 (bottom) under SYN-synchronous (light grey line) and SV-spatially variable (black line) input. The theoretical SDOF amplification curve is also reported (dashed line).

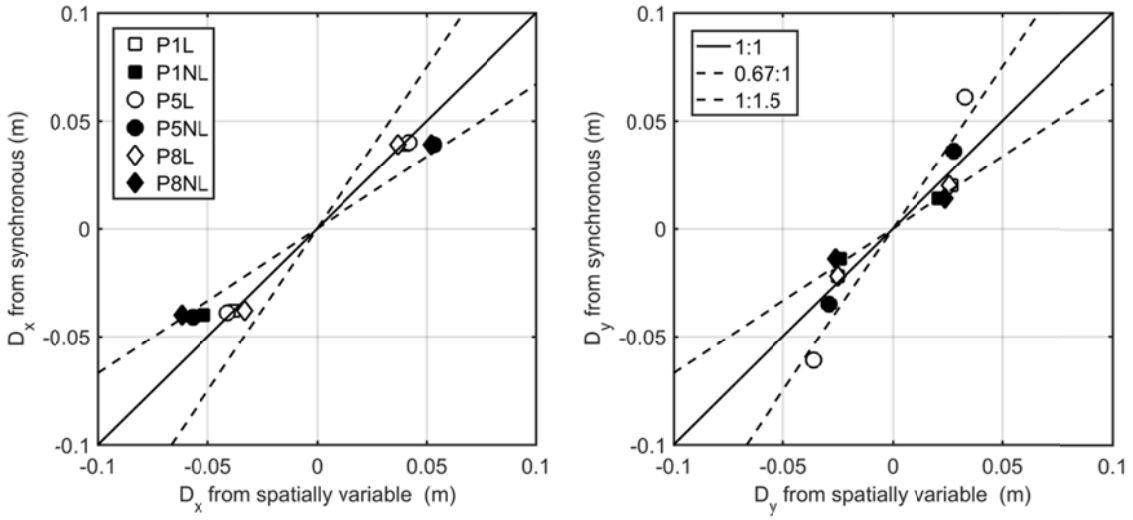

Figure 7 Deck relative displacement maxima along the longitudinal X (D_x, left) and transverse Y (D_y, right) direction, from SV analysis, on the *x*-axis; and SYN analysis, on the *y*-axis, for piers P1, P5 and P8. White and black markers refer to linear and non-linear analyses, respectively.

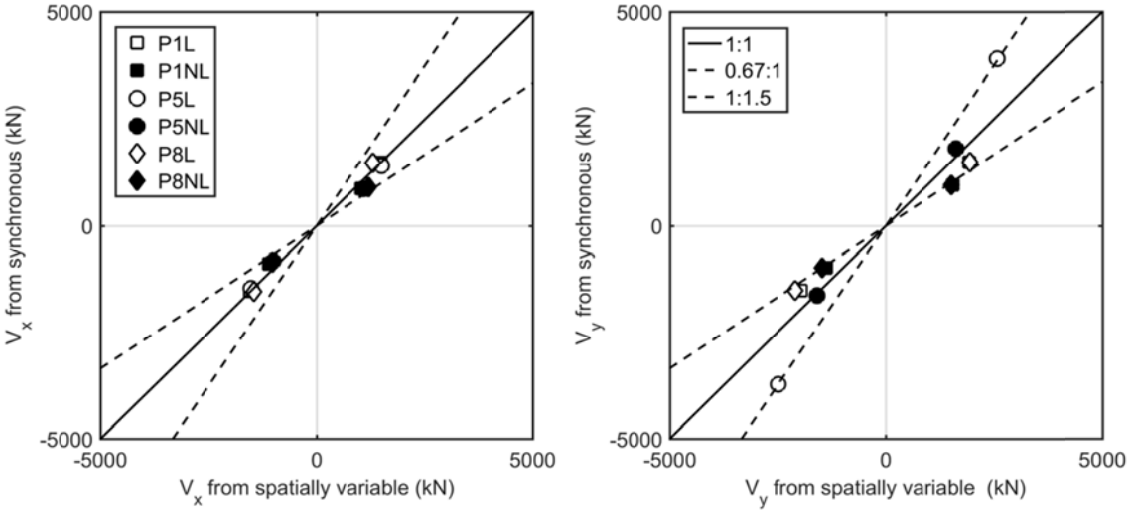

Figure 8 Same as in Figure 7 but for pier shear forces along the longitudinal X (V_x, left) and transverse Y (V_y, right) direction.

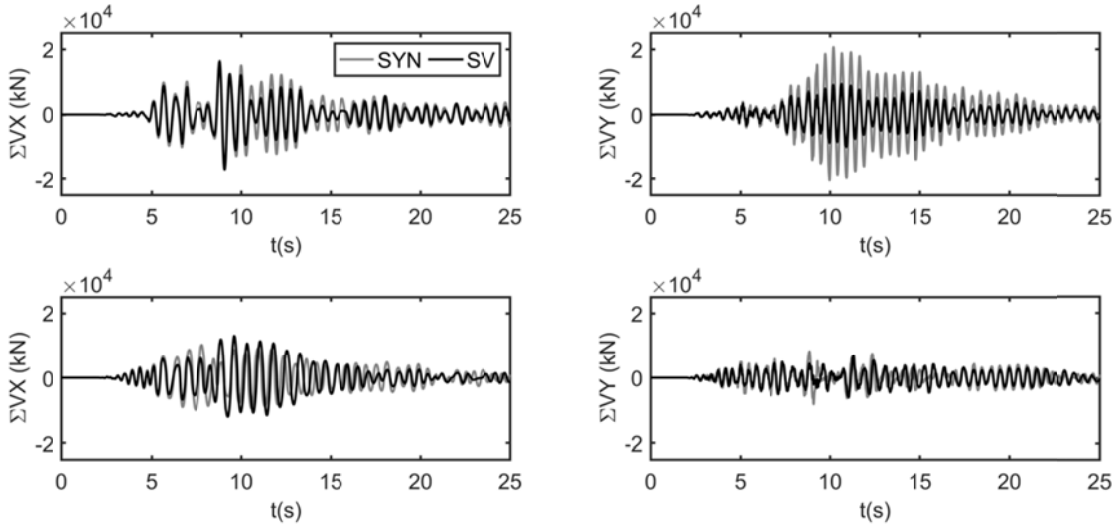

Figure 9 Time histories of longitudinal (left) and transverse (right) base shear from SYN (light grey line) and SV (black line) analyses for both linear (top) and non-linear (bottom) behavior.

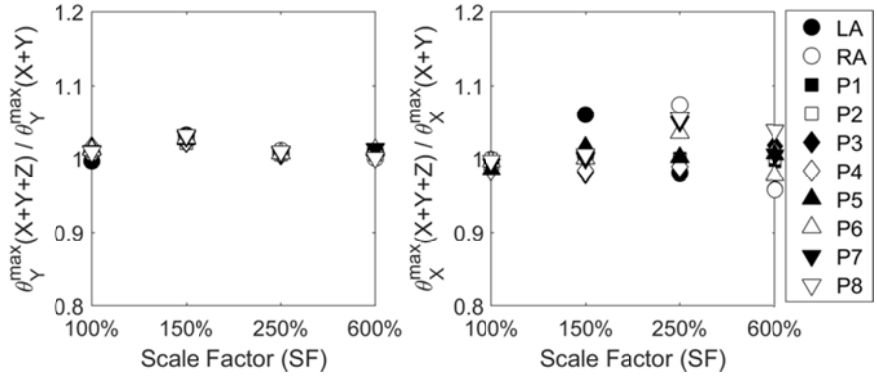

Figure 10 Ratio of maximum chord rotations θ^{max} (left: around Y; right: around X) from three-directional input (X+Y+Z) over those from bi-directional horizontal motion (X+Y) as a function of scale factor of IDA.

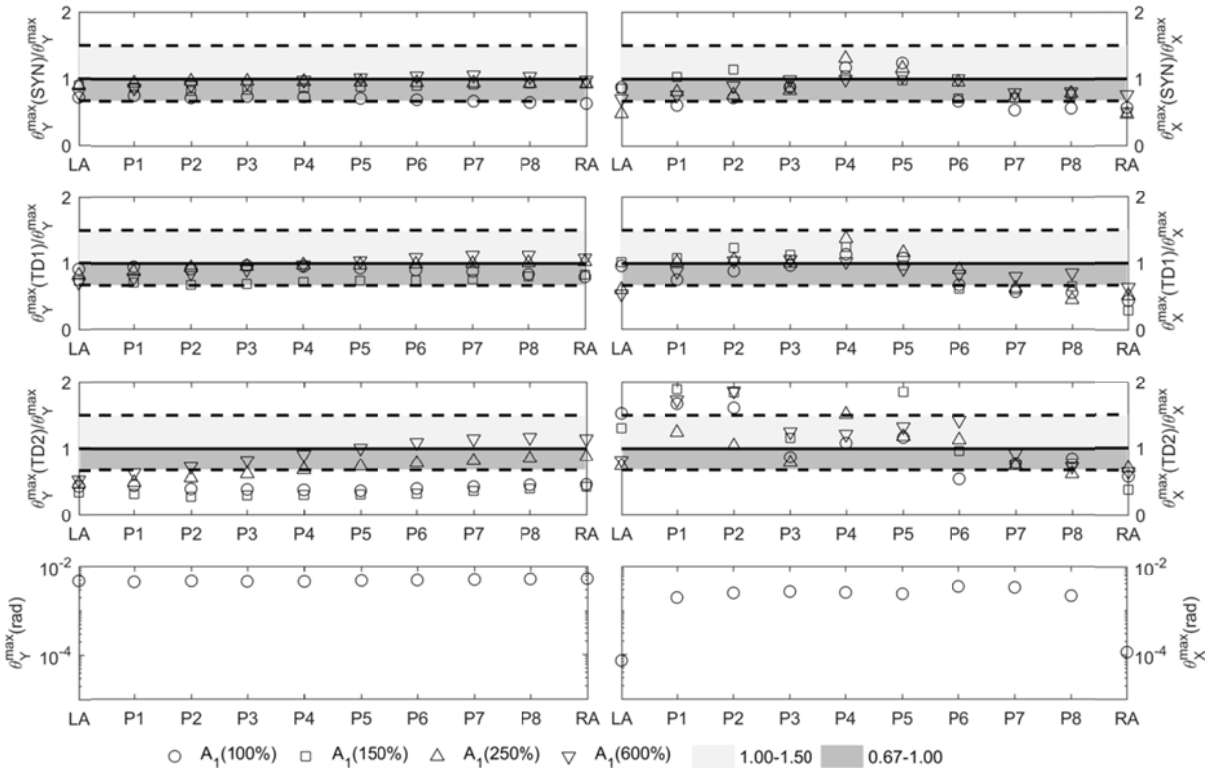

Figure 11 Ratio of maximum chord rotations θ^{max} (left: around Y; right: around X) obtained from SYN analysis, TD analysis with V_{a1}=2400 m/s (TD1) and V_{a2}=1000 m/s (TD2), over those from SV analyses (case of alignment A1). The absolute values of θ^{max} from SV analyses are shown in the bottom panel.

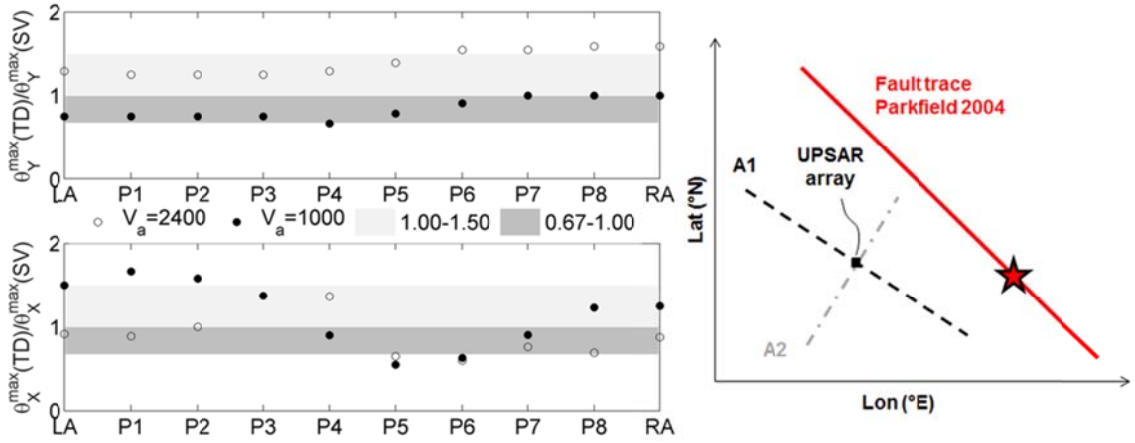

Figure 12 Left: ratio of θ^{max} from TD analyses with V_{a1}=2400 m/s (white dots) and V_{a2}=1000 m/s (black dots) over the one from SV analyses, under the assumption of record set A2=S08-S09-S10. Right: orientation of two alignments with respect to seismic fault of Parkfield earthquake.

Appendix A

As a further task, the seismic performance of the bridge has been assessed for different EC8 limit states through IDA, where the input ground motions has been incrementally scaled for both SYN and SV case. According to Eurocode 8- Part 3, §2.2 [CEN, 2005b], performance-based assessment of the bridge under consideration (regular RC structure of "normal" importance) has been carried out for damage limitation (DL), significant damage (SD) and near-collapse (NC) limit states, corresponding to the return periods T_r=225, 475 and 2475 years, respectively. For completeness, the relevant equations of EC8-Part 3 (§A.3.2 in Annex A "Reinforced Concrete Structures") for the estimation of chord rotation capacity (θ) and shear resistance (V) for the different limit states are reported below (see also Table A1). Note that DL, SD, and NC limit states correspond to a chord rotation limit represented by yield chord rotation (θ_y), 0.75 of ultimate chord rotation capacity (θ_{um}), and ultimate chord rotation capacity, respectively.

The chord rotation capacity (θ_{um}) is defined as follows:

$$\theta_{um} = \frac{1}{\gamma_{el}} 0.016 \left(0.3^{\nu}\right) \left(\frac{\max\{0.01, \omega'\}}{\max\{0.01, \omega\}} f_c \right)^{0.225} \left(\min\{9, L_V / h\}\right)^{0.35} 25^{\left(\alpha \rho_{sx} \frac{f_{yw}}{f_c}\right)} 1.25^{100 \rho_d} \quad \text{(A1)}$$

where: γ_{el} is a structural element based coefficient, =1.5 (primary seismic elements) and =1.0 (secondary seismic elements), h is the depth of cross-section, L_V = M/V is the ratio moment/shear at the end sections (known as shear span), $\nu = N/bhf_c$ (b: width of compression zone, N: axial force positive for compression), ω (ω') is the mechanical reinforcement ratio of the tension (compression) longitudinal reinforcement, f_c and f_{yw} are the concrete compressive strength (MPa) and the stirrup yield strength (MPa) respectively, ρ_{sx} is ratio of transverse steel parallel to the direction x of loading, ρ_d is the steel ratio of diagonal reinforcement in each diagonal direction, α is the confinement effectiveness factor (readers are referred to Eurocode 8 - Part 3, A.3.2.2 for further details of calculation α).

The value of the plastic part of the chord rotation capacity can be estimated as follows:

$$\theta_{um}^{pl} = \theta_{um} - \theta_y = \frac{1}{\gamma_{el}} 0.0145 \left(0.25^{\nu}\right) \left(\frac{\max\{0.01, \omega'\}}{\max\{0.01, \omega\}} \right)^{0.3} f_c^{0.2} \left(\min\{9, L_V / h\}\right)^{0.35} 25^{\left(\alpha \rho_{sx} \frac{f_{yw}}{f_c}\right)} 1.275^{100 \rho_d} \quad \text{(A2)}$$

where, θ_y is the chord rotation at yielding and rest of the variables are defined in Eq. (A1). Yield chord rotation for columns and walls can be computed using Eqs. (A3) and (A4), respectively.

$$\theta_y = \phi_y \frac{L_V + a_v z}{3} + 0.0014\left(1 + 1.5\frac{h}{L_V}\right) + \frac{\varepsilon_y}{d - d'}\frac{d_b f_y}{6\sqrt{f_c}} \quad \text{(A3a)}$$

$$\theta_y = \phi_y \frac{L_V + a_v z}{3} + 0.0014\left(1 + 1.5\frac{h}{L_V}\right) + \phi_y \frac{d_b f_y}{8\sqrt{f_c}} \quad \text{(A3b)}$$

$$\theta_y = \phi_y \frac{L_V + a_v z}{3} + 0.0013 + \frac{\varepsilon_y}{d - d'}\frac{d_b f_y}{6\sqrt{f_c}} \quad \text{(A4a)}$$

$$\theta_y = \phi_y \frac{L_V + a_v z}{3} + 0.0013 + \phi_y \frac{d_b f_y}{8\sqrt{f_c}} \quad \text{(A4b)}$$

where: ϕ_y is the yield curvature of the end section, $a_v z$ is the tension shift of the bending moment diagram (z is the length of internal level arm, a_v=1 if shear crack precedes flexural yielding at the end section, otherwise a_v=0), f_y and f_c are the steel yield stress and the concrete strength respectively, $\varepsilon_y = f_y/E_s$ (E_s: elastic modulus of the steel), d and d' are the depths to the tension and compression reinforcement respectively, d_b is the mean diameter of the tension reinforcement.

The shear strength (V_R) can be computed as follows:

$$V_R = \frac{1}{\gamma_{el}}\left[\frac{h - x}{2L_V}\min\{N, 0.55A_c f_c\} + \left(1 - 0.05\min\{5, \mu_\Delta^{pl}\}\right)\left(0.16\max\{0.5, 100\rho_{tot}\}\left(1 - 0.16\min\{5, L_V/h\}\right)\sqrt{f_c}A_c + V_W\right)\right] \quad \text{(A5)}$$

where: γ_{el} is equal to 1.15 and 1.0 for primary and secondary seismic elements respectively, x is the compressive zone depth, N is the compressive axial force (positive), A_c is the cross-section area, ρ_{tot} is the total longitudinal reinforcement ratio, V_W is the contribution of transverse reinforcement to shear resistance ($V_w = \rho_w b_w z f_{yw}$, being ρ_w: transverse reinforcement ratio, b_w: width of the core concrete, z: length of the internal level arm, f_{yw}: yield stress of the transverse reinforcement), L_V is the shear span, h is the depth of the cross-section, μ_Δ^{pl} is the plastic part of the ductility demand.

In case maximum shear span ratio (L_V/h) of a column is less or equal than 2.0, then, its shear strength can not exceed $V_{R,max}$, which corresponds to the value of failure by web crushing as defined in Eq. (A6). For walls, on the other hand, $V_{R,max}$ is given by Eq. (A7).

$$V_{R,\max} = \frac{\frac{4}{7}\left(1 - 0.02\min\{5, \mu_\Delta^{pl}\}\right)}{\gamma_{el}}\left(1 + 1.35\frac{N}{A_c f_c}\right)\left[1 + 0.45\left(100\rho_{tot}\right)\right]\sqrt{\min\{40, f_c\}}\, b_w z \sin(2\delta) \quad \text{(A6)}$$

$$V_{R,\max} = \frac{0.85\left(1-0.06\min\{5,\mu_{\Delta}^{pl}\}\right)}{\gamma_{el}}\left(1+1.8\min\{0.15,{}^{N}\!/_{A_c f_c}\}\right)\left(1+0.25\max\{1.75,100\rho_{tot}\}\right)\left[\left(1-0.2\min\{2,L_V/h\}\right)\sqrt{f_c}\,b_w z\right] \quad \text{(A7)}$$

where, δ is the angle between the diagonal and the axis of the column (as $\tan\delta = h/2L_v$). The rest of the variables are explained in the Eq. from (A1) to (A5).

To determine the elastic design spectrum specific for the target site, we considered the Uniform Hazard Spectrum (UHS) estimated for the HBMC site by USGS (https://earthquake.usgs.gov/hazards/interactive/) for return periods T_r=225, 475, and 2475 years, assuming stiff soil conditions, i.e., V_{S30} (shear wave velocity in the top 30 m)=360 m/s. Then, the input motions at the bridge base nodes are linearly scaled in time domain by a scale factor of 1.5, 2.5 and 6, such that the response spectrum of "mean" gm7 matches reasonably well the target UHS within the range of modal periods (i.e. T=0.2s-0.6s), see Figure A1.

The overall results of performance assessment considering both SV and SYN motion are provided in Table A2. It can be noted that no significant change in the performance states are observed due to asynchronous motion, apart from change from II to III for the NC limit state (T_r=2475 years) in the abutment level, for which the presence of backfill-abutment interaction was neglected. As a matter of fact, although not documented herein for sake of brevity, the latter is found to have a beneficial effect owing to the presence of passive backfill pressure.

To analyze in greater detail the effects of spatial variability on the non-linear response of the bridge, the moment-chord rotation (M-θ) hysteresis loops at selected piers (P1 and P5) are shown in Figure A2. It can be observed that the hysteretic paths show significant similarity essentially with a change in the peak demand. Consistently with previous analyses (see Section 5.2), rotational demands around X axis (i.e. associated with transverse response of the bridge) are found to be increasing in end-span (P1) piers and decreasing in mid-span piers (P5), when SV input is considered.

Table A1 Summary of the criteria for performance-based assessment according to Eurocode 8 Part 3 – Annex A [CEN, 2005b]. DL: Damage limitation, SD: Significant damage, NC: Near collapse.

Structural Element	Chord Rotation			Shear
	DL	SD	NC	NC
Rectangular beams and columns (*pier*)	(A3a) or (A3b)	0.75xNC	(A1) or (A2) + (A3a) or (A3b)	(A5) and (A6)
Rectangular walls (*abutment*)	(A4a) or (A4b)		0.58 x (A1) or 0.60 x (A2) + (A3a) or (A3b)	(A5) and (A7)

Table A2 Results of performance-based assessment. I: below yield rotation, II: between yield rotation- ¾ of ultimate rotation capacity, III: Between ¾ of ultimate rotation capacity to rotation capacity.

IDA	100%	150% (T_r=225 y)	250% (T_r=475 y)	600% (T_r=2475 y)
SYN	I	II	II	II
SV	I	II	II	III

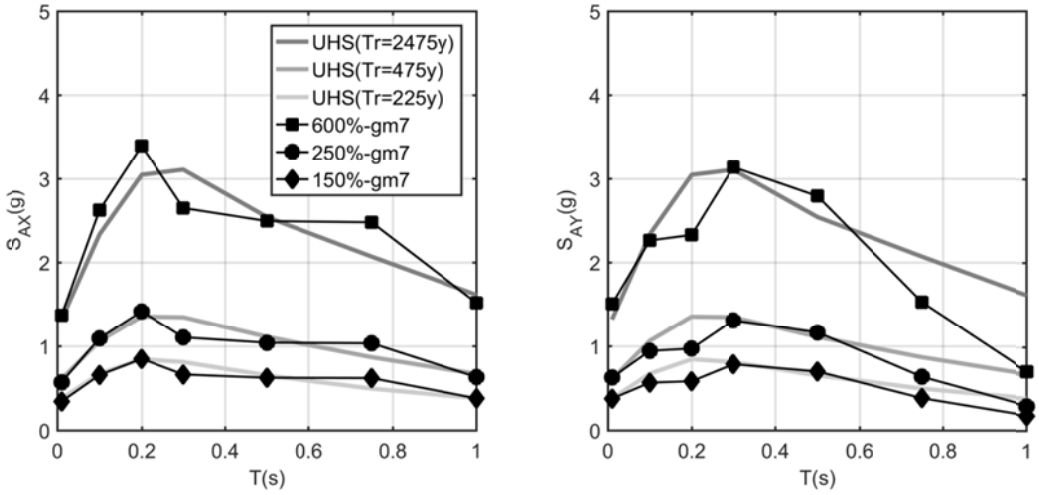

Figure A1 Uniform Hazard Spectra (UHS) and response spectra of linearly scaled gm7 (1.5, 2.5 and 6 scale factors) in the range of periods of major interest for structural response (left: longitudinal direction, right: transverse direction).

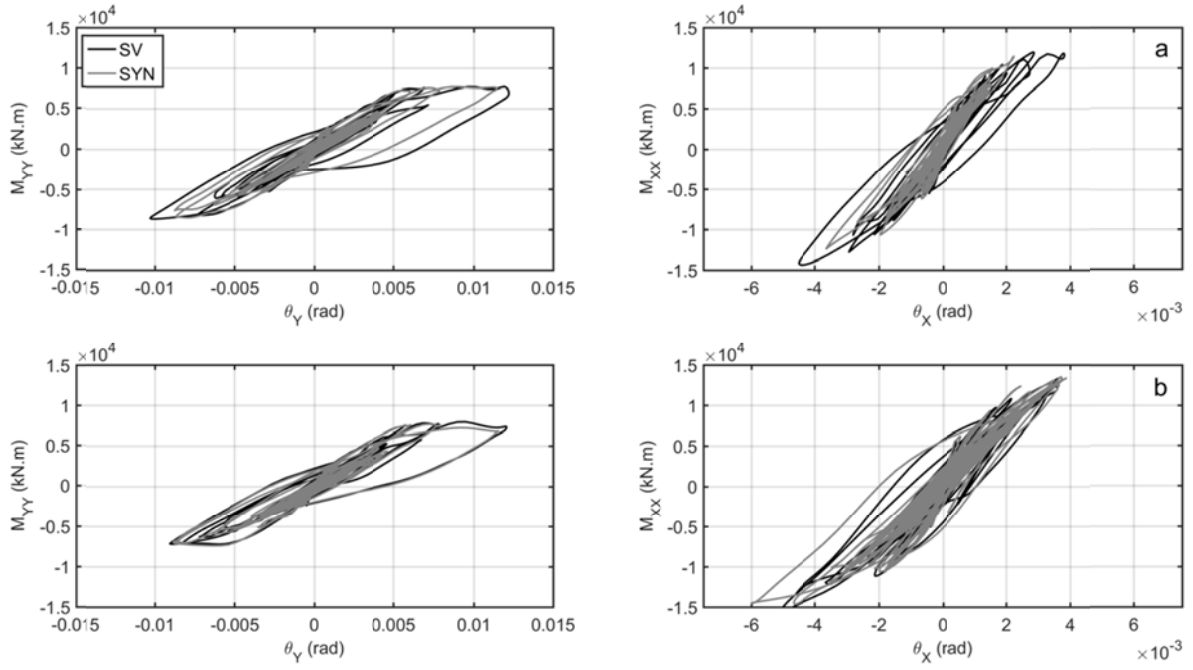

Figure A2 Moment (*M*)-chord rotation (*θ*) curves from SYN (light grey line) and SV (black line) analyses (left: bending around Y, right: bending around X) for piers P1 (a) and P5 (b), from IDA with scale factor=2.5.